Journal of Structural Geology, Vol. 9, No. 5/6, pp. 719 to 730, 1987
Printed in Great Britain

0191-8141/87 $03.00 + 0.00

Preferred orientation of phyllosilicates in phyllonites and ultramylonites

DAVID K. O'BRIEN* and H.-R. WENK

Department of Geology and Geophysics, University of California, Berkeley, CA 94720, U.S.A.

LOTHAR RATSCHBACHER†

Institut für Geologie und Paläontologie, Universität Graz, 8010 Graz, Austria

and

ZHENDONG YOU

Beijing Graduate School, Wuhan College of Geology, Beijing, People's Republic of China

(*Received* 7 *April* 1986; *accepted in revised form* 3 *February* 1987)

Abstract—X-ray texture goniometry operated in the transmission mode has been applied to fine-grained, phyllosilicate-rich *SC*-mylonites from the Santa Rosa mylonite zone (California), the Whipple Mountains core-complex (California), and the Austroalpine nappes of the Eastern Alps (Austria). Basal planes (00*l*) phyllosilicate pole-figures depart in two respects from orthorhombic symmetry. (a) The maximum pole density deviates from the pole to the mylonitic foliation and lies along a great circle which is normal to the foliation and contains the mylonitic lineation, and (b) the contours of equal pole density are more widely spaced on one side of the (00*l*)-maximum than on the other measured along the mylonitic lineation. Optical microscopy reveals *S*- and *C*-surfaces and sets of shear bands (SB) characteristic of non-coaxial deformation. The pole figures are used for two purposes. (a) The first is strain estimation after the March model by imposing orthorhombic symmetry. The resulting March strains are more or less the same in all Californian samples. This is interpreted as evidence for a 'steady state foliation'. (b) The second is shear sense determination. It is demonstrated that consistently asymmetric preferred orientations reflect structures which are typical of non-coaxial deformation. It is concluded that X-ray analysis of phyllosilicate-rich mylonites can, in addition to providing an estimate of total strain, give information about deformation regime and shear sense. Furthermore, the study documents the heterogeneous nature of deformation on macroscopic and microscopic scales, and the importance of non-coaxial deformation in accommodating large strains.

INTRODUCTION

ZONES OF intense crustal deformation containing mylonites have become of great current interest (e.g. Tullis *et al.* 1982). The mechanisms of mylonite formation are still controversial. Are they a result of cataclastic or ductile deformation? How important is the component of non-coaxial strain? Are compositional factors significant in the local concentration of deformation? In this paper we wish to address aspects of the latter two questions and explore how X-ray texture analysis can be used to analyze ultramylonites and phyllonites of granitic and sedimentary origin that are too fine-grained to be readily investigated by conventional petrographic methods. It would be particularly useful to know: (a) if and how the method of March (1932) (see Oertel 1983, 1985) for strain determination applies to highly deformed rocks; and (b) how structures such as *S*- and *C*-surfaces and shear bands (Berthé *et al.* 1979, Platt & Vissers 1980, White *et al.* 1980, Simpson & Schmid 1983, Platt 1984), which have become extremely useful indicators of deformation regime and shear sense, are expressed in the preferred orientation of phyllosilicates. For a general discussion of fabric asymmetry the reader is referred to Bouchez *et al.* (1983).

We concentrate on rocks from the Santa Rosa mylonite zone in southern California. This 100 km-long belt of deformation along the eastern margin of the Peninsular Range batholith is, to our knowledge, one of the largest, most intensely deformed and best exposed mylonite zones. It serves as the type area for our preferred orientation studies and strain determinations after the March theory. The results from the Santa Rosa mylonite zone study are then applied in studies of two other mylonite zones of current interest: mylonites along the detachment faults of the Whipple mountain core complex in SE California (Davis *et al.* 1980) and along thrusts of the Upper Austroalpine nappes in the Eastern Alps of Austria (Ratschbacher 1986).

STRUCTURAL SETTING

Santa Rosa mylonite zone

The Santa Rosa mylonite zone is the northern portion of the eastern Peninsular Ranges mylonite zone, which

*Present address: Hawaii Institute of Geophysics, University of Hawaii, Honolulu, Hawaii 96822, U.S.A.
†Present address: Geologisches Institut, Universität Tübingen, 7400 Tübingen, F.R.G.

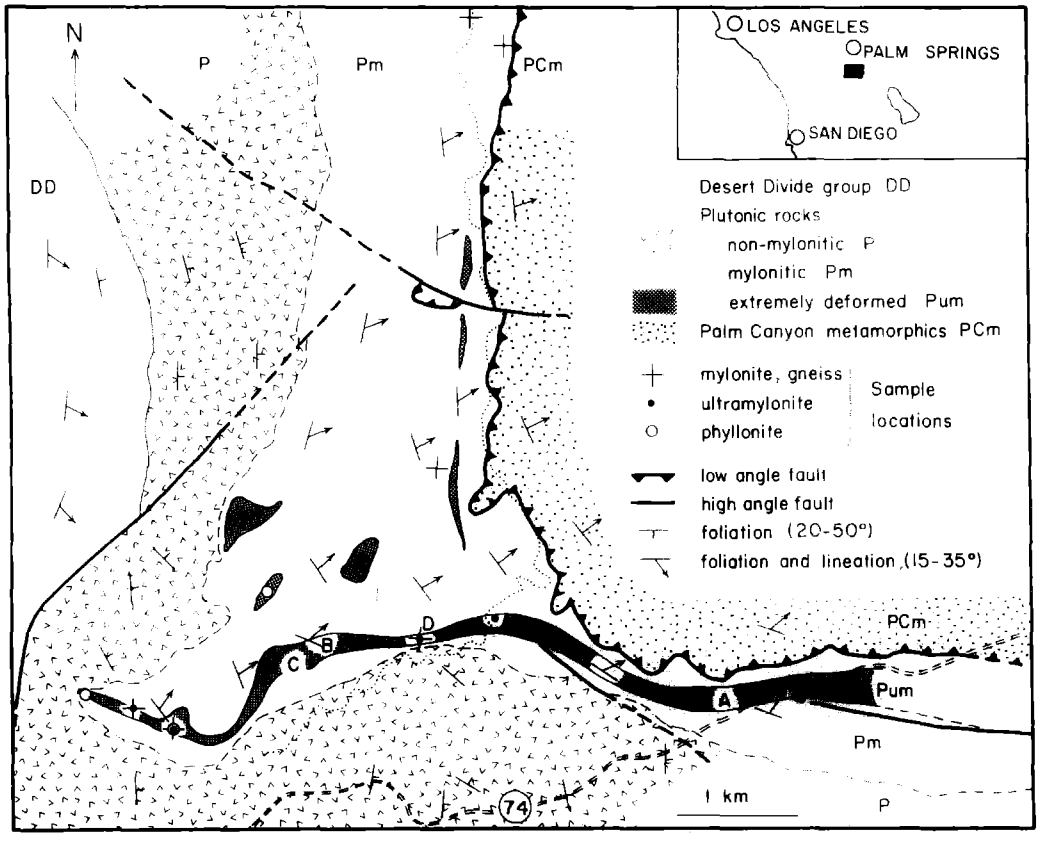

Fig. 1. Geologic-tectonic map of upper Palm Canyon (Santa Rosa mylonite zone), California. The locations of samples for chemical analyses are indicated by crosses, dots and circles. ABCD indicate localities of specimens used in textural studies. Highway 74 and the stream in Palm Canyon (dots) are shown for reference (from Erskine 1985).

borders the Cretaceous northern Peninsular Ranges batholith in southern California (Sharp 1979). The sequence of mylonitic plutonic and metasedimentary-tectonites is cut by a sequence of at least five imbricate low-angle faults. The structurally lowest belt of rocks represents mylonitized orthogneisses which grade into their relatively undeformed plutonic counterparts below. Field evidence and available isotopic constraints suggest that deformation of the batholith accompanied the later stages of magmatic intrusion and continued through Late Cretaceous to Early Tertiary uplift of the batholith (Erskine & Wenk 1985).

Whipple Mountains

The Whipple Mountains of southern California belong to a distinctive group of metamorphic terrains along the axis of the North American Cordillera known collectively as metamorphic core complexes (Crittenden *et al.* 1980). Although details of the mechanism of deformation are controversial, it is generally accepted that the core complexes define a belt of crustal thinning postdating Sevier and Laramide compressional tectonics but predating late Tertiary Basin-and-Range extension and rifting. Rocks comprising the core complex consist of gently-dipping, pervasively foliated and lineated mylonitic gneisses and related rocks. They are truncated by the Whipple detachment fault which is responsible for the emplacement of a cover terrain of non-mylonitic rocks (Davis *et al.* 1980).

Upper Austroalpine nappes

The Upper Austroalpine nappes (Tollmann 1959) constitute the tectonically uppermost units of the Alps. The sampled rocks are part of two major thrust systems, the Graywacke Zone and the Gurktal Nappe in east-central Austria. Their structural evolution is characterized by non-coaxial deformation associated with west-directed thrusting and ductile flow within the nappes followed by north–south shortening by folding and fold imbrication (Ratschbacher 1986). In the investigated samples, structures of the first deformation event are well preserved. The deformation was accompanied by recrystallization at conditions ranging from middle to upper greenschist facies and is of Cretaceous age (e.g. Ratschbacher & Klima 1985, Von Gosen *et al.* 1985).

DEFORMATION STRUCTURES

Santa Rosa mylonite zone

Samples were collected in the upper Palm Canyon area (Fig. 1) where particularly good exposures of heterogeneously deformed granitic rocks are present below the Palm Canyon Fault. In most places it separates the plutonic part of the Santa Rosa mylonite zone from an upper unit consisting mainly of metamorphic rocks which were metamorphosed to high-grade amphibolite facies during the igneous activity. The plutonic tecto-

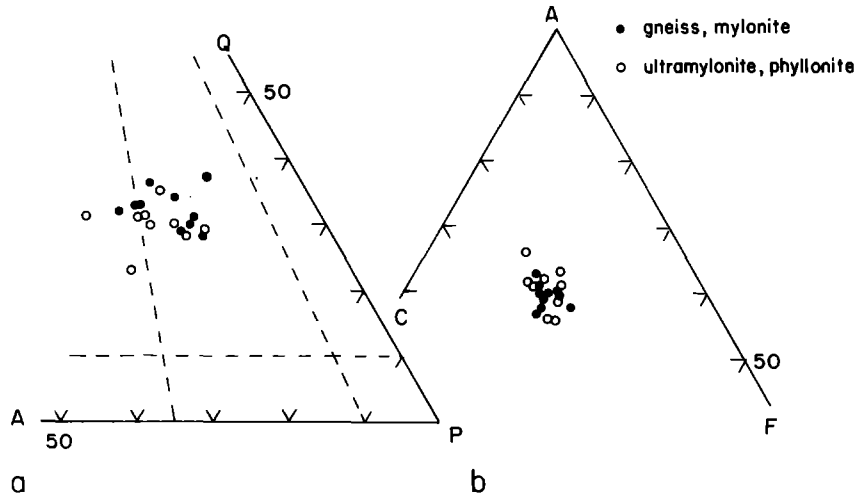

Fig. 2. QAP and ACF diagrams for deformed plutonic rocks from upper Palm Canyon. Hornblende–biotite norms were calculated from XRF analyses.

nites consist of augen gneisses, mylonites, ultramylonites and phyllonites (we use the term phyllonite here as originally defined by Sander 1911, p. 301 and Knopf 1931, p. 20, which does not imply retrograde metamorphism). They are characterized by a well-developed mylonitic, east-dipping foliation and a northeasterly-plunging stretching lineation. Ultramylonite and phyllonite sequences range in thickness from 1 cm to 50 m. Post-deformational folding of the region has produced a large flexure in the upper Palm Canyon, part of which is shown in Fig. 1 (from Erskine 1985).

Ultramylonites are generally black, dense rocks resembling pseudotachylites, whereas phyllonites are light brown in color and possess a well-developed cleavage, giving them a slaty appearance. Both contain high concentrations of phyllosilicates. We analyzed the chemical and mineralogic composition of samples with different degrees of deformation by X-ray fluorescence and powder diffraction. Results for major components are illustrated on QAP and ACF diagrams in Fig. 2. Although some compositional variation is present on these plots, no consistent pattern can be discerned. Trace elements in mylonites and granodiorites of Palm Canyon are also essentially identical, demonstrating that compositional variations found in the mylonitic rocks are inherited from their parents. The average normative composition is 28% quartz, 17% alkali feldspar, 43% plagioclase and 6% biotite, as is typical of granitic rocks. A similar mineralogical composition was ascertained by X-ray powder patterns, and no significant increase in biotite, chlorite or quartz content could be found with progressive deformation. In contrast to mylonites and phyllonites, ultramylonites contain significant concentrations of epidote (O'Brien 1985), which accentuates the mylonitic lineation. We conclude that mylonitic deformation is an isochemical process even though considerable recrystallization occurs.

In most of our samples, we observe in sections cut parallel to the mylonitic lineation and perpendicular to the dominant foliation two or more sets of roughly planar surfaces, which are schematized in Fig. 3. The mylonitic, often wavy foliation is defined by compositional banding, particularly of quartz and asymmetric tails of feldspar porphyroclasts. In Fig. 3 we refer to this as '*S*-foliation'. Waviness of *S* is due to shear zones which cut across *S* at irregular intervals and extend the rocks along the mylonitic lineation. These shear zones, termed '*C*-cleavage' in Fig. 3, have a *constant orientation across the whole mylonite zone.* They are defined by the preferred orientation of grain shapes along them and they constitute the dominant surface in all highly deformed rocks (mylonites, phyllonites, ultramylonites). A third set of surfaces, termed 'shear bands' (SB) in Fig. 3, is poor in quartz and, assuming dextral shear as a reference, is inclined 25° to the *C*-cleavage, leading to an additional component of extension along the mylonitic lineation. Biotite flakes within SB are themselves inclined 5–7° to the trace of SB. These SB structures are usually less than one mm thick and irregularly spaced (3–10 mm). The photomicrographs of Fig. 4 provide an overview of the *S*–*C*–SB structures (see caption).

We interpret the planar surfaces in terms of non-coaxial deformation following Berthé *et al.* (1979), Platt & Vissers (1980) and White *et al.* (1980). We corroborate

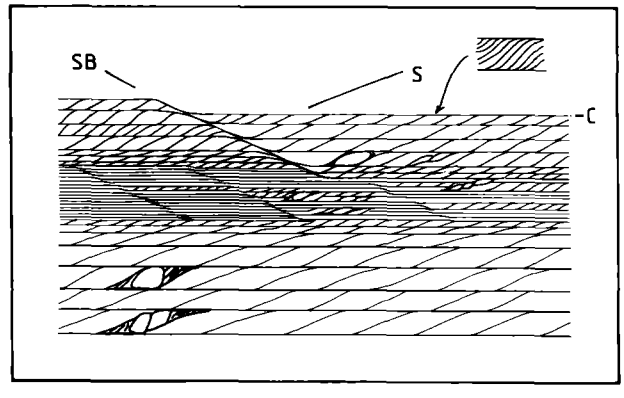

Fig. 3. Schematic drawing illustrating the various surfaces in the Santa Rosa mylonites. *S*, schistosity; *C*, cleavage; SB, shear band.

this interpretation of an overall deformation involving a component of simple shear by the presence of the following features observed and measured in our samples: coherent rotated clasts (e.g. feldspar and quartz) with sigmoidal shadows (Fig. 4c & d), some asymmetry in fabrics of quartz (Erskine 1985), and plane strain qualitatively read from a three-dimensional analysis of pressure shadows. The shear sense is consistently upper plate toward the southwest.

We examined in detail one sample of ultramylonite, six samples of phyllonite and three samples of moderately deformed mylonite from each of four different areas, labeled A, B, C and D on Fig. 1. At locality A, phyllonites occur as minute bands up to 2 mm thick, surrounded by well-lineated mylonite in proximity to the contact with undeformed plutonic rocks.

At locality B, phyllonites form an unusually thick zone (15m), which resembles an exposure of slate, especially at the top where no lineation is present. Recrystallized quartz grains have a strong crystallographic orientation of *c*-axes roughly parallel to the foliation plane and normal to the lineation, as can be demonstrated by the insertion of the gypsum plate. Samples are fine-grained and unusually homogeneous. *C*-surfaces are the dominant planar element, but *S*-domains are still preserved in quartz rich layers and shear bands (SB) are numerous as well (Fig. 4a). Note the offset (arrow in Fig. 4a) in a quartz-rich layer aligned parallel to *C*. A traverse through the zone was sampled to document variations in texture.

At locality C, a 10 m thick phyllonite zone shows wavy bands (Fig. 4b) contrary to the situation at other localities where the bands are more or less planar (Fig. 4a). Quartz and biotite grains are dominantly elongated parallel to the *S*-foliation (Fig. 4c). There are also porphyroclasts of feldspar and quartz and quartz lenses within the biotite-rich matrix. Some of the lenses and most of the porphyroclasts are elongated parallel to the *S*-foliation, with the exception of their tails which curve into parallelism with the *C*-planes (Fig. 4d).

The ultramylonite was sampled at locality D. Porphyroclasts of quartz, feldspar, epidote and euhedral sphene are in general oriented parallel to the *S*-foliation (Fig. 4e). Grain size is larger than in the phyllonites.

In nearly all of the investigated samples *S*- and *C*-planes have rotated into near coincidence. The composite foliation is best defined by alignment of quartz grains into bands. At high magnification, the individual biotite grains in quartz-rich bands are seen to be inclined at 5–20° counterclockwise from the *C*-cleavage (Fig. 4c), assuming again dextral shear as reference. This is the same angle that the asymmetric quartz and feldspar porphyroclasts within the fine-grained matrix are inclined to the *C*-cleavage (Fig. 4c–e). A further characteristic feature of the rocks is the presence of narrow quartz-poor domains whose traces are approximately linear, discontinuous and inclined at about 25° clockwise to the *C*-cleavage (note that they are inclined in the opposite sense to the biotite in the quartz-rich areas). The biotites within the quartz-poor domains are not parallel to the domain boundaries but are inclined anticlockwise at 5–7° to these boundaries (Fig. 4f). The quartz-poor domains are the shear bands.

Microstructures in several samples were examined with the transmission electron microscope. Diffraction patterns of phyllosilicates are generally streaked parallel to c^* (Fig. 5 inset), particularly along rows $k \neq 3n$ typical of the 1M polytype (Bell & Wilson 1981) with (001) stacking faults. Sometimes it is possible to detect spots corresponding to the chlorite (004) *d*-spacing of 7.04 Å, suggesting local chlorite–biotite intergrowths. Qualitative X-ray analysis of the phyllosilicate mineral in the electron microscope shows that it is predominantly composed of Si, Al, K, Ca, Mg and Fe with a trace of Ti, which identifies it as biotite rather than muscovite. Microstructures of associated quartz always display features of recovery with ubiquitous dislocation networks, indicating that deformation occurred at elevated temperatures.

Whipple Mountains

Samples were collected at the 'mylonitic front' about 5 km southwest of Whipple Peak (fig. 6 in Anderson *et al.* 1979) where the mylonite belt plunges moderately to the southwest, exposing its upper contact with non-mylonitic crystalline basement rocks. Ultramylonites and phyllonites are generally restricted to discrete bands up to 1 m in thickness. Ultramylonitic layers, faults, and tight asymmetric interfolial folds, as well as porphyroclasts of quartz and feldspar and bands of quartz, are present in thin sections. Biotite grain size is $\leq$ *ca* 0.02 mm, and the biotite flakes appear inclined counterclockwise 15–25° to the mesoscopic foliation, again with a dextral shear sense assumed as reference.

Upper Austroalpine nappes

The investigated rocks show a pronounced planolinear (*LS*) fabric and are from different vertical positions within single nappes (Ratschbacher 1986). Specimen SE55 just overlies a major discontinuity in the thrust system of the Graywacke Zone. This quartz–chlorite–mica mylonite (Fig. 6a) shows quartz-rich layers, in which pronounced grain growth occurred, and mica–quartz domains. The mesocopic mylonitic schistosity is composed of *S*- and *C*-surfaces, which are nearly coincident. Specimen B19 is a mica–chlorite–quartz phyllonite from the interior of the same thrust sheet as SE55; it shows a dominant *C*-cleavage, relict *S*-foliation, and irregularly spaced shear bands (Fig. 6b). Specimen GD17, a mica–quartz mylonite, overlies the basal thrust of the Gurktal thrust system and reveals *C*-cleavage extended by shear bands (Fig. 6c).

Six samples from the same or nearby outcrops contain pebbles which can be used to estimate strain. Pebble strains lie along the plane-strain line or in the constrictional field (Fig. 7), thus confirming the interpretation of an overall deformation with a major component of simple shear (Ratschbacher 1986).

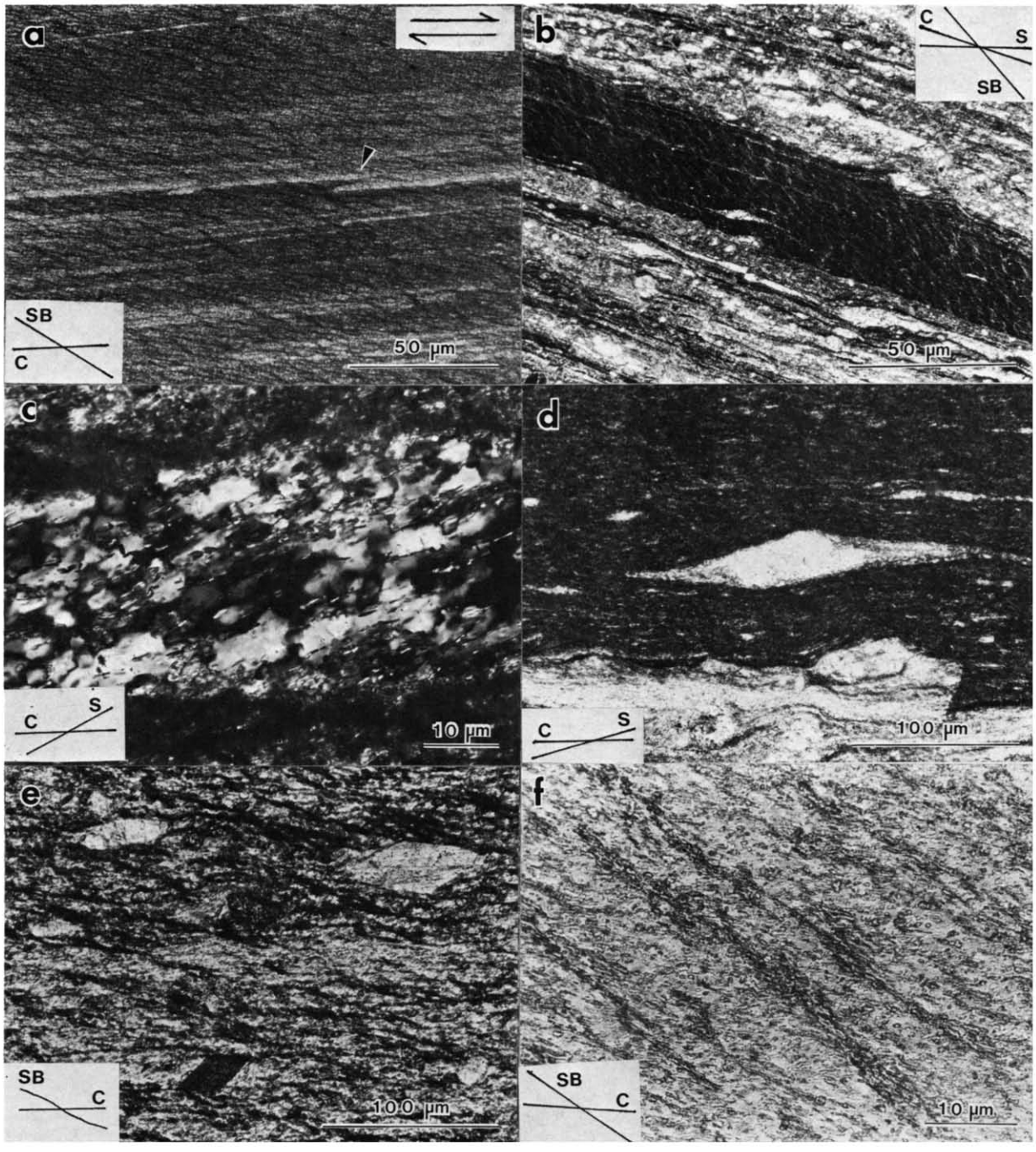

Fig. 4. Photomicrographs and diagrammatic representation of planar surfaces in phyllonitic, mylonitic and ultramylonitic rocks of the Santa Rosa mylonite zone. Samples are cut parallel to lineation, and perpendicular to foliation. Shear sense is dextral. (a) Phyllonite sample B6 in crossed polars. Note faults in quartz-rich layers (arrow). The dark lines at an angle to the *C*-surfaces are the quartz-poor domains of the shear bands. (b) Sample C2 of a thin phyllonite band in mylonitic rock in crossed polars. Quartz-poor shear bands are prominent as light lines at an angle to the *S*-foliation. (c) Quartz-rich layer in sample C5 containing elliptical quartz grains and biotite grains that are parallel to the *S*-foliation. Crossed polars with mica plate inserted. (d) Asymmetric augen of quartz tilted back against the sense of shear, with tails of finer grained material parallel to the *C*-surfaces in sample C2 under plane polarized light. (e) Sphene porphyroclast (dark and euhedral) and two plagioclase porphyroclasts (light) tilted against the sense of shear in sample D1; plane polarized light, biotite grains are parallel to the *S*-foliation in strain shadows and less deformed elliptical pods. (f) Dark quartz-poor domains (shear bands) of phyllonite sample B6 in crossed polars with mica plate inserted. The biotite grains in the quartz-rich regions are wavy, as in a crenulation cleavage.

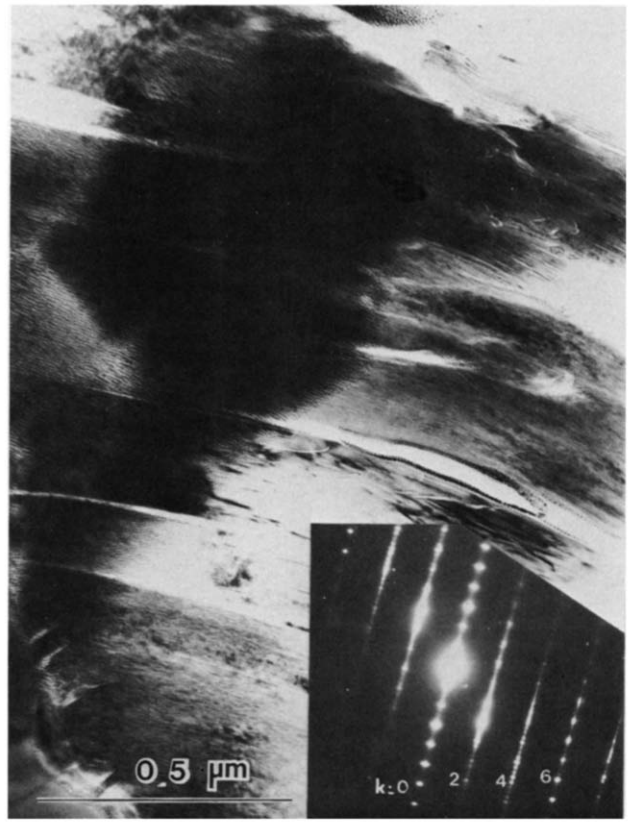

Fig. 5. Bright field TEM micrograph of moderately bent biotite in Santa Rosa phyllonites. Inset at lower right is a diffraction pattern that documents stacking disorder along c^*.

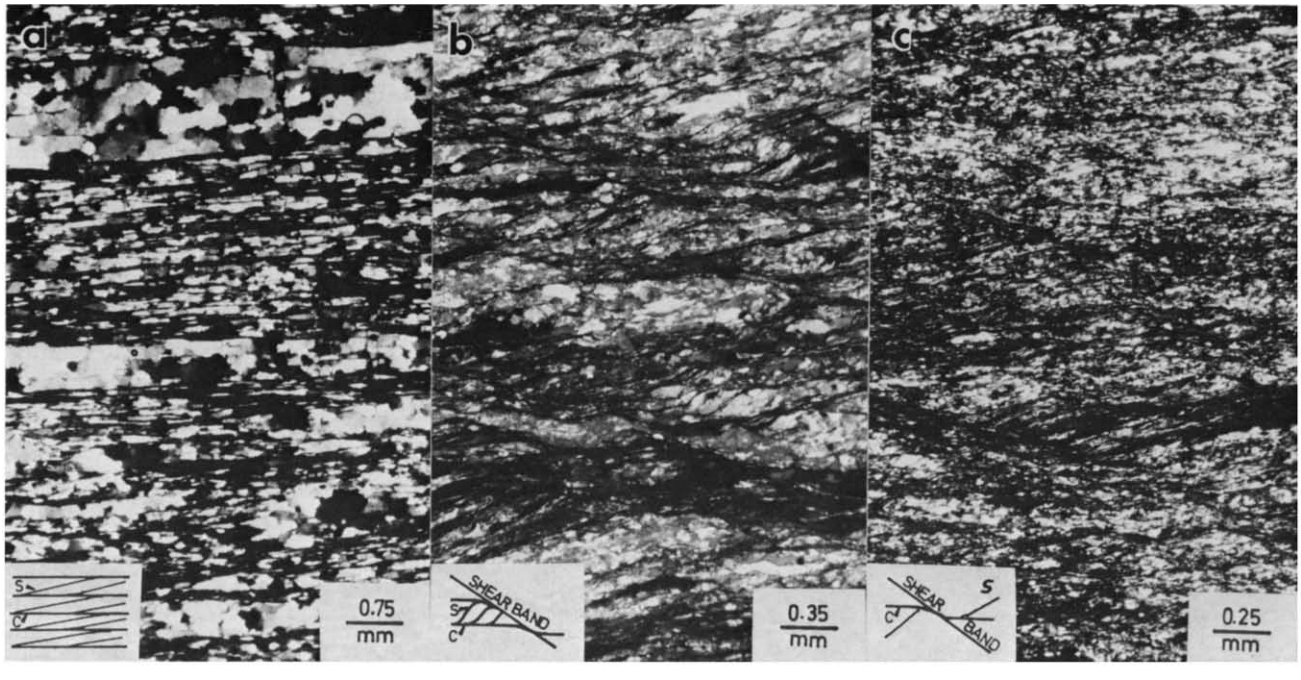

Fig. 6. Photomicrographs and diagrams to illustrate the orientations and mutual relationships of different sets of planar surfaces in mylonitic metasediments of the Upper Austroalpine nappes of Austria. (a) SE55; (b) B19; (c) GD17.

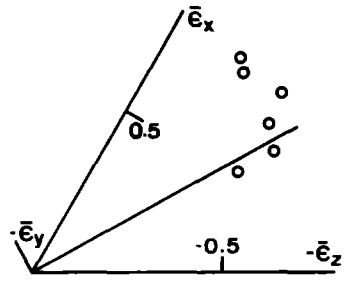

Fig. 7. Three-axis plot of pebble strains measured from the same or nearby outcrops of the samples collected in the Austroalpine nappes of the Eastern Alps. $\bar{\varepsilon}$: natural strain; $X \geq Y \geq Z$: principal strain axes.

PREFERRED ORIENTATION

Pole figures of phyllosilicates of most samples from the Santa Rosa mylonite zone and from the Whipple Mountains were measured at the University of California, Berkeley. The X-ray data collection and processing methods for the construction of a pole figure have been described in detail by O'Brien (1985). The method is a modification of the one described by Oertel (1983) and Wenk (1985), and a few comments are appropriate here for those who may wish to use similar methods in their laboratories. Two 100 μm thick sections were cut perpendicular to the foliation from each sample, one parallel to the lineation (section A) and one perpendicular to the lineation (section B). Biotite (001) reflections corresponding to d = 10Å in these sections were then scanned in transmission mode with a Phillips pole figure goniometer applying Cu Kα radiation. X-ray intensities were counted for 50 sec. The pole figure was scanned in concentric small circles spaced at 5° up to a tilt of 40° (pole distance ϱ = 50°). At higher angles the beam defocusing effect and absorption of X-rays by the sample became too strong to be corrected satisfactorily. Most of the missing data were collected from a scan over the second section, and then the two data sets were overlapped. It took about 27 h to measure a complete pole figure from two thin sections.

The data were collected, processed, and plotted using a microcomputer. The processing program subtracts the background intensity and corrects for defocusing and absorption. The background for section A was first arbitrarily chosen as the average of the minimum X-ray counts of the scan which contained the texture peak, usually at a 0° tilt of the goniometer cradle. Then the ratio of texture peak intensity to background intensity was determined. After section B was scanned, its background was determined by dividing its texture peak intensity by the peak-to-background ratio of section A. This compensated for the slight differences in thickness between the two sections. The two sections were now compatible for overlapping. The background for biotite cannot be determined in the traditional way with a 2Θ scan because it has been determined that the apparent background near the (001) peak is not independent of texture. The 'anisotropy of background' is attributed to the fact that the background is due not only to incoherent scattering and fluorescence but also to diffraction on (00l) lattice planes of biotite with a variable d-spacing caused by stacking disorder (Fig. 5, inset).

All samples from the Eastern Alps and a few samples for comparison from the Santa Rosa mylonite zone were investigated at the University of California, Los Angeles (UCLA). Instead of biotite, chlorite (002) reflections corresponding to d = 14Å (SE55, GD17) and muscovite (002) reflections corresponding to d = 10Å (B19, SE55) were measured in the samples from the Alps. Data collection and processing methods for these samples strictly followed the technique described by Oertel (1983).

Table 1. Pole densities (ϱ), March strains (ε), and inclination of direction of maximum pole density to pole of C-cleavage for phyllosilicate basal plane pole figures of samples discussed in this study

Sample	Rock type	$\varrho_1(\perp C)$	ϱ_2 (in m.r.d.)	$\varrho_3(\parallel l)$	ε_1	ε_2 (March, $\Delta l/l_0$)	ε_3	Inclination (°)
Santa Rosa mylonite zone (Fig. 1)								
A1*	mylonite	3.69	0.57	0.48	−0.35	0.21	0.28	0
B6	phyllonite	18.03	0.37	0.15	−0.62	0.39	0.89	2
B8	phyllonite	23.62	0.33	0.13	−0.65	0.46	0.97	4
B9	phyllonite	15.25	0.40	0.16	−0.60	0.35	0.83	3
B9*	phyllonite	9.39	0.35	0.30	−0.53	0.42	0.49	1
B10	phyllonite	18.81	0.37	0.15	−0.62	0.40	0.90	2
C3	phyllonite	16.01	0.39	0.17	−0.60	0.37	0.81	5
C5	phyllonite	16.14	0.36	0.17	−0.60	0.40	0.80	2
C5*	phyllonite	13.45	0.32	0.23	−0.58	0.46	0.63	15
D1	ultramylonite	13.53	0.39	0.19	−0.58	0.37	0.74	2
Whipple Mountains								
WM2	ultramylonite	22.50	0.35	0.13	−0.65	0.42	0.99	4
WM3	ultramylonite	16.05	0.39	0.16	−0.60	0.37	0.84	1
Eastern Alps								
SE55 (musc.)*	mylonite	9.38	0.83	0.12	−0.53	0.06	0.98	+8
B19 (musc.)*	mylonite	17.29	0.53	0.10	−0.61	0.23	1.1	−4
GD17 (chl.)*	mylonite	6.99	0.65	0.21	−0.48	0.15	0.66	−8

*Asterisk denotes UCLA measurements.

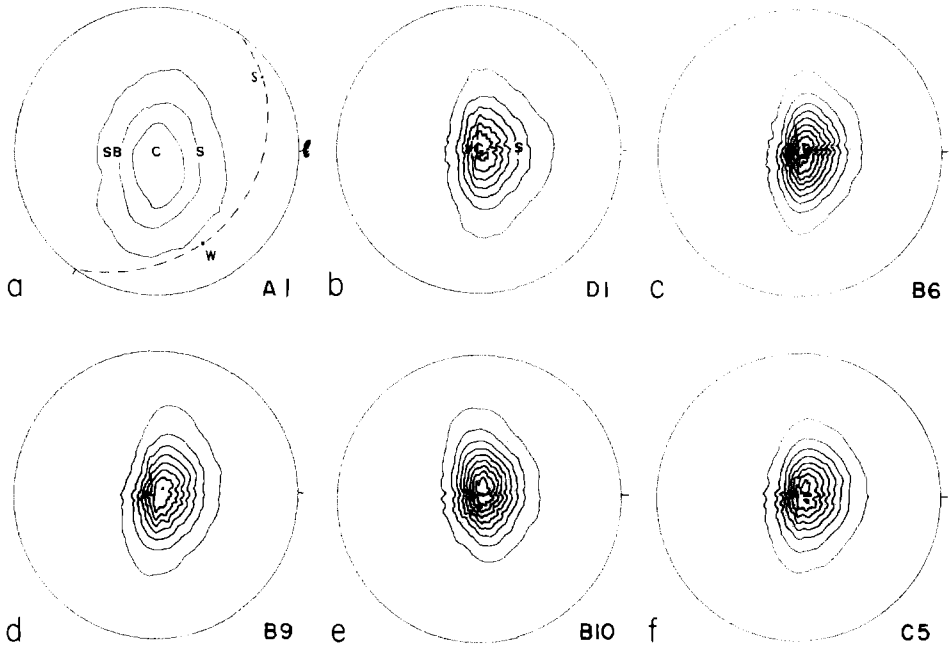

Fig. 8. Biotite (001) pole figures from the Santa Rosa mylonite zone projected on the macroscopic *C*-surface. *l* is extension lineation. Dashed line defines horizontal plane with W = West and S = South. All equal-area projections, lower hemisphere. (a) A1 mylonite (maximum of 3.7 m.r.d.). (b) D1 ultramylonite (max. of 13.5 m.r.d.). (c)–(f) phyllonites: (c) B6 (max of 18.0 m.r.d.); (d) B9 (max. of 15.2 m.r.d.); (e) B10 (max. of 18.8 m.r.d.); (f) C5 (max. of 16.1 m.r.d.). Contours for (a) at 1, 2 and 3 m.r.d.; for (b)–(f) at 1, 3, 5, 7, 9, 11, 13 and 15 m.r.d. Pole to *C*-cleavage, *S*-surface and SB shear band are indicated by letters. All samples are more or less in the same geographic orientation (*C* cleavage is NE-dipping). All measurements done at Berkeley except for (a), which was done at UCLA.

The corrected X-ray intensities were then normalized to express pole densities ϱ in multiples of a random distribution (m.r.d.) and represented on a sphere. The pole figures were plotted in equal-area projection (lower hemisphere) with the pole to the '*C*-cleavage', the most constantly oriented element of the mylonite zone, coinciding with the center, and the down-dip lineation direction at the left (northeast in the case of the Santa Rosa samples).

Pole figures of sample C5 (Table 1) were measured both at Berkeley and at UCLA, using slightly different experimental set-ups and methods of data reduction, and the results are very similar. The contour lines of measured equal pole density approximate concentric ellipses stretched out along a girdle normal to the mylonitic lineation and foliation (Figs. 8–10). The maximum and minimum (001) pole densities plot near the *C*-plane normal and near the lineation, respectively. However, the pole maximum is off-center to the pole of the *C*-cleavage (projection center), and the intensity contour spacing is asymmetric along the direction of the mylonitic lineation.

The method of Oertel (1983, 1985) was used to determine March strains $\varepsilon_i = \Delta l/l_0$ from pole densities ϱ_i in the principal fabric directions assuming homogeneous deformation and orthorhombic fabric symmetry. The values for ϱ_i, ε_i, and angles between the center of the concentric ellipses and the pole to the macroscopic *C*-plane ('inclination') for all samples are presented in Table 1.

POLE FIGURE DATA: RESULTS AND INTERPRETATION

March strains

The March strains calculated from the different Santa Rosa phyllonite samples are strikingly similar (Table 1 and Fig. 8c–f), which suggests a homogeneous distribution of strain throughout the rock as well as low strains. Both are unlikely considering the different deformation intensities our samples represent. We conclude that the development of preferred orientation progressed until an equilibrium was reached corresponding to what has been proposed by Means (1981) as a 'steady-state folia-

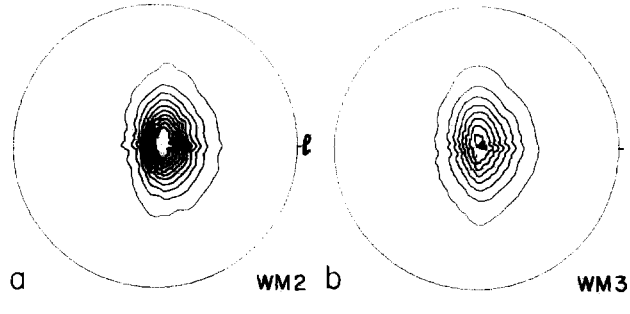

Fig. 9. Biotite (001) pole figures from Whipple Mountain mylonites. Projection plane is parallel to the *C*-cleavage plane. All equal-area projections. (a) WM2 (max. of 22.5 m.r.d.); (b) WM3 (max. of 16.0 m.r.d.); contours at 1, 3, 5, 7, 9, 11, 13, 15, 17 and 19 m.r.d. *l* is lineation.

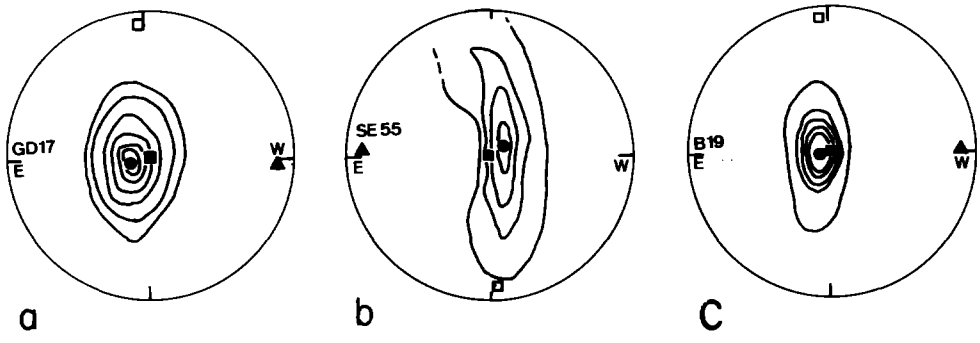

Fig. 10. Phyllosilicate pole figures of samples from the Austroalpine nappes projected on the *C*-cleavage. The solid circle, open square and solid triangle, are the maximum, intermediate and least pole densities, the solid square is the plot center and *C*-cleavage pole. Mylonitic lineation is E–W and shear sense is upper plate toward W. (a) GD17 phyllonite, chlorite (002), contours at 1.5, 2, 3, 4, 5 and 6 m.r.d. (max. of 7.0 m.r.d.). (b) SE55 mylonite, muscovite (002), contours 1, 2, 4 and 6 m.r.d. (max. of 9.4 m.r.d.). (c) B19 mylonite, muscovite (002), contours at 1, 3.5, 6, 8.5 and 11 m.r.d. (max. of 17.3 m.r.d.).

tion' on the basis of theoretical considerations. According to Means *et al.* (1984), most of the micas in their experimentally deformed samples were expected to be in an equilibrium orientation for sample shortenings greater than 90%. This limits the application of the March model for very highly strained rocks, and we suggest that an equilibrium preferred orientation of biotite corresponding to a steady-state foliation had been reached in all our Santa Rosa phyllonite and ultramylonite samples. Preferred orientation is significantly weaker in the Santa Rosa mylonites than it is in the phyllonites and ultramylonites (Fig. 8a). Interestingly, preferred orientation in ultramylonites from the Whipple Mountain core-complex is similar to that in the Santa Rosa phyllonites (Table 1, Fig. 9). By contrast, March strains from the Austroalpine mylonites are comparatively low and variable (Table 1, Fig. 10). Larger March strains than those calculated by Means *et al.* (1984) and those determined in the present work have been reported by Rumble & Oertel (1979) in schists from New Hampshire. This suggests that the limiting strains for the March model may vary with lithology.

Pole-figure asymmetry

The maxima in Santa Rosa biotite (001) orientations (lower hemisphere projections) are consistently inclined toward the southwest at an average angle of 4° from the pole to the '*C*-cleavage' towards the lineation. The steeper slope of the pole distribution is always on the side pointing against the shear sense. We illustrate these asymmetries in sample B6, a Santa Rosa phyllonite, using a scan of the texture peak at a 0° tilt of the goniometer cradle on a section cut parallel to the lineation and normal to the *C*-plane (Section A) and compare it with a Gaussian distribution of the same halfwidth (25°) (Fig. 11a). The measured peak is slightly steeper than the Gaussian, and if we superpose the two curves so that they coincide at half height the asymmetry of the texture peak becomes evident.

We propose that biotite grains, preferentially disposed along *S*-, *C*- and SB-surfaces, produce three single distributions, which add up to form the asymmetric total distribution. An example of a bimodal distribution corresponding to *S*- and *C*-surfaces is shown in Fig. 11(b) for phyllonite sample B6, in which it is possible to measure (001) cleavage-traces on an enlarged photomicrograph. The histogram displays two maxima separated by 12°. In the individual measurements we can only discern rather large grains and have to assign to each an average orientation, which is the reason for the rather sharply defined subdistributions (Fig. 11b). In the X-ray scan we average over the whole volume, including bent portions of crystals, and the distributions become more

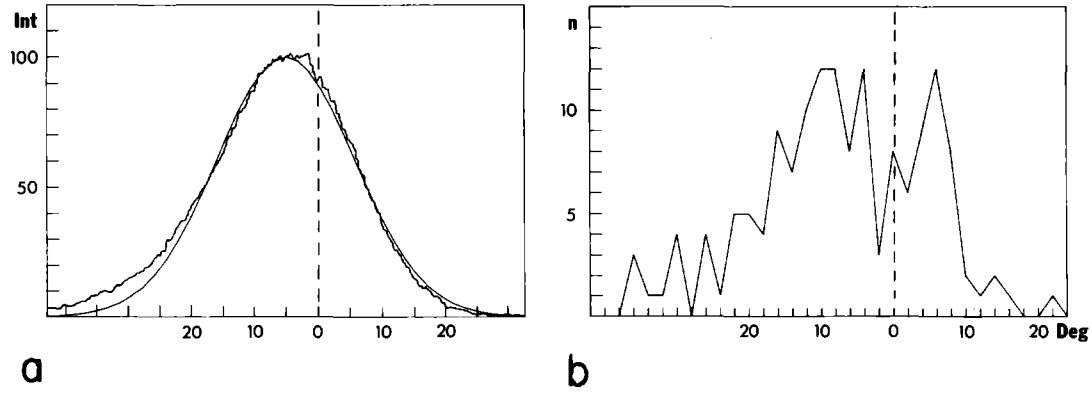

Fig. 11. Profiles across the texture peak of Santa Rosa mylonite sample B6. (a) Biotite (001) X-ray scan and fit of Gaussian curve. Note the asymmetry. (b) Histogram of biotite (001) orientations measured as traces on an enlarged photograph parallel to lineation and normal to the *C*-cleavage.

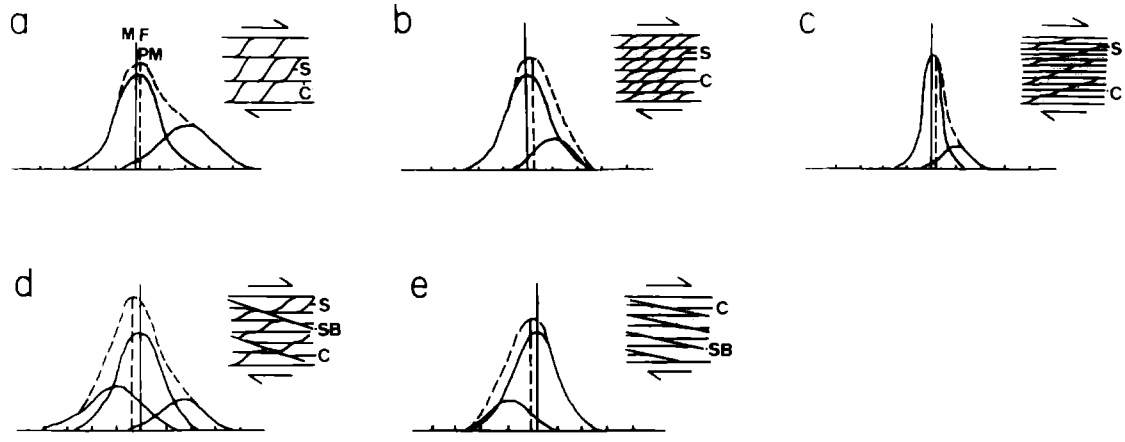

Fig. 12. Interpretation of peak asymmetry as bi- and trimodal distributions. Hypothetical cumulative intensity profiles (stippled line) obtained by combination of profiles inferred from theoretical preferred phyllosilicate orientations of *S*- and *C*-surfaces and one set of shear bands (solid lines). Diagrammatic illustration of orientations and mutual relationships of foliations constituting the intensity profiles. S: *S*-surfaces; C: *C*-surfaces; SB: shear bands; MF: pole to *C*-cleavage; PM: pole distribution maximum. Models correspond to (a) Fig. 8b; (b) Figs. 8c–f and 9a & b; (c) Fig. 10b; (d) Figs. 8a and 10a; (e) Fig. 10c.

diffuse, coalescing into a single asymmetric peak (Fig. 11a).

The side of the steeper slope of the pole distribution (e.g. Fig. 11a) depends on: (a) the intensity of development of the different planar surfaces and thus the strength of the subdistributions; and (b) the angle between the different sets of planar surfaces. In the case of the Santa Rosa mylonites, this is the angle between the foliation normal given by the distribution maximum of the *C*-surface pattern and that determined by the *S*-surface pattern.

Figure 12(a & b) are theoretical histograms of orientation traces of the subdistributions, the resulting total distributions, and their interpretation as bimodal distributions simulating the pole figures of the Santa Rosa mylonite zone. In weakly deformed mylonites and augen gneisses, when *S*-surfaces are clearly distinguishable from *C*-surfaces even in hand specimens, resolution of the X-ray analysis is limited by the coarse grain size of both phyllosilicates and non-phyllosilicates, which results in poor grain statistics even if a translation device is used (Lipshie *et al.* 1976). However, due to the high angle between the *S*- and *C*-surface sets in this case the pole figure asymmetry and slope differences of the intensity profiles (Fig. 12a) are most accentuated. In zones of high strain or when a component of coaxial deformation is present (Erskine & Wenk 1985, Ratschbacher 1986), the foliation plane (*S*) nearly coincides with the shear plane (*C*), making the angle between them and thus the pole figure asymmetry and slope difference very small. In thin sections, non-coaxial deformation may still be indicated by asymmetric pressure shadows behind occasionally preserved rigid objects and relicts of *S*- and *C*-surfaces in lozenge-shaped domains of minor deformation. This stage, which is characteristic of most of the fine-grained biotite-rich mylonites, corresponds to the ultramylonite stage of Berthé *et al.* (1979). The X-ray pole figures corresponding to this stage give a reliable indication of the particular submicroscopic structures and the shear sense both from the position of the maximum and the asymmetry of the texture peak.

A critical point for the analysis of structures and shear sense is the consistent choice of an appropriate reference frame. In our samples, the *C*-surface set was used throughout because of its penetration on all scales and its consistent orientation within the entire deformation zone.

The pole figures from the phyllonites and ultramylonites of the Whipple Mountains (Fig. 9) are similar to those of the Santa Rosa mylonite zone (Fig. 8) and are interpreted accordingly. The mylonites and phyllonites of sedimentary origin of the Austroalpine nappes provide evidence for much larger variation in texture than the California samples. They also illustrate that some care should be given to shear sense interpretation. The pole figure of sample SE55 (Fig. 10b) is nearly identical to those from the Santa Rosa mylonites; however the *C*-surface subdistribution is extremely sharp, and *S*-surfaces are weakly developed, as shown in thin section and represented in Fig. 12(c). In the other two specimens the development of numerous, irregularly spaced, and about 0.1 mm wide shear bands (SB) is observed. These bands penetrate the *S*- and *C*-surfaces (Fig. 6b & c). The deformation is extremely heterogeneous on the scale of the sample. In the corresponding X-ray pole figure (Fig. 10c) the effect of the shear bands is to move the pole maximum in a direction 'opposing' the shear (Fig. 12d). However, the pole figure asymmetry is similar to the Santa Rosa mylonites with respect to the sense of shear. But when shear bands are extensively developed and when *S*-surfaces are subordinate, as in sample B19 (Fig. 6b), the asymmetry of pole maximum and slope becomes opposite to that of the California samples with respect to the sense of shear (Figs. 10c and 12e). In this situation, and as indicated by the visible microstructures, the anisotropy introduced by the *C*-surfaces and developed during the earlier stages of deformation may be disrupted by the anisotropy of the shear bands. This may

lead to an opposite asymmetry and hence to a misinterpretation of the shear sense.

DISCUSSION

The specimens studied here provide information about deformational microstructures in fine-grained, phyllosilicate-rich mylonites that are generally difficult to examine by optical microscopy.

Deformation of relatively homogeneous isotropic rocks, such as large plutons, under a nearly constant strain rate may result in the development of wide zones of homogeneous deformation. Homogeneous strain is typically portrayed by nearly orthorhombic phyllosilicate pole-figures (e.g. Oertel 1970). A sudden increase in strain rate across a zone of deformation, such as due to an overall extension, may concentrate deformation in macroscopic 'shear bands', which may weaken the material. In the case of the Santa Rosa mylonite zone (1–5 km wide), extreme deformation is concentrated in narrow bands (13–15 m wide) which are irregularly distributed over the more highly strained portion of the mylonite zone. The deformation in the larger zone is mainly attributed to crustal thinning under pure shear conditions, which is responsible for the *S*-foliation planar structure (Erskine & Wenk 1985). Simple shear was probably predominant in the formation of ultramylonites and phyllonites. This is indicated by the development of mainly one set of penetrative 'shear bands' (*C*-cleavage) with a systematic asymmetry with respect to the *S*-plane. At this stage, in the fine-grained, biotite-rich tectonites, X-ray pole figures typically display textures with asymmetric pole maxima and intensity profiles which give a reliable indication of non-coaxial deformation and shear sense. In a later stage, the previously established anisotropy is overprinted by a second set of shear bands (SB) that occur as minute bands in the ultramylonitic layers and occasionally as wide bands in mylonites.

Layered sedimentary rocks, such as those in the Austrian Alps, may be deformed heterogeneously from the onset of deformation. This is due to the inherited heterogeneous nature of layering and the different threshold temperatures for activation of plastic deformation mechanisms of the principal minerals in the layers (Voll 1980, Ratschbacher 1986). Strain rates are thus locally extremely variable and the heterogeneity of deformation on all scales is evidenced by complicated microstructures and textures.

The textures in some of our rocks are reminiscent of those resulting from heterogeneous deformation during large strain in metals to produce shear bands with localized strain concentrations (e.g. Mecking 1978). They are thought to be the result of instabilities developed during softening. In all three study areas, increasing overall deformation results in grain-size reduction, to some extent by cataclasis (feldspar and phyllosilicates), but mainly by syntectonic recrystallization (quartz and phyllosilicates).

CONCLUSIONS

Biotite (002) pole figures have been measured from ultramylonites and phyllonites of the Santa Rosa mylonite zone and the Whipple Mountains core complex, California. They are all remarkably consistent in their asymmetry, being steeper towards the down-dip lineation direction (NE) and off-center with respect to the normal to the *C*-cleavage by about 4° to the southwest, resulting in a monoclinic symmetry. This is different from fabrics commonly observed in slates and schists in which strain seems to be homogeneously distributed and for which orthorhombic symmetry is observed.

These pole figures are used for two purposes. First, applying the model of March (1932) and imposing orthorhombic symmetry, the three principal March strains of the rocks were estimated. They are more or less the same in all samples, and are relatively low. As the existence of a homogeneous state of strain in rocks with different deformation intensities distributed over a large area is unlikely, this has been interpreted as evidence for a 'steady state foliation' (Means 1981). The March strain values here represent only a lower limit of the actual strains.

The pole figures are also used for sense of shear determinations. The asymmetry of the pole figures is here demonstrated to be the result of microstructures indicative of non-coaxial deformation: ubiquitous *S–C* surfaces and local shear bands (SB). Since the pole to the main mylonitic planar structure, considered to be parallel to the *C*-shear planes, does not coincide with the center of the biotite (002) pole intensity maximum we infer a dominant *S–C* surface geometry (Berthé *et al.* 1979), and therefore a sense of shear can be determined as upper plate directed toward the southwest. This sense is consistent with the one obtained from observations of asymmetric porphyroclasts (Simpson & Schmid 1983).

Asymmetric chlorite and muscovite (002) pole figures from the Austroalpine nappes of the Eastern Alps are interpreted in a similar manner. However, they portray a larger variation in microstructures (*S–C* surfaces and shear bands) reflecting higher heterogeneity of deformation in stratified lithologically variable sedimentary rocks.

The study emphasizes the heterogeneous nature of deformation from macroscopic to submicroscopic scale and the importance of non-coaxial deformation in accommodating large strains.

Acknowledgements—We thank G. Oertel for access to his texture goniometer at UCLA, where some of the pole figure measurements were made, and for stimulating discussion and interest in this work. Research of L.R. at UCLA was supported by grant 5251 of the Oesterreichische Forschungsfonds, the Fulbright Foundation and the Syrian government. H.R.W. acknowledges support through NSF grant EAR-84-06070. We are appreciative of discussions both in the field and laboratory with B. Erskine and L. Goodwin and greatly indebted for constructive criticism offered by the reviewers, particularly W. D. Means.

REFERENCES

Anderson, J. L., Davis, G. A. & Frost, E. G. 1979. Field guide to regional Miocene detachment faulting and early Tertiary mylonitic terranes in the Colorado river trough, Southeastern California and Western Arizona. In: *Geological Excursions in the Southern California Area* (edited by Abbott, P. L.). San Diego State University, 109–133.

Bell, I. D. & Wilson, C. J. L. 1981. Deformation of biotite and muscovite: TEM microstructure and deformation model. *Tectonophysics* **78**, 201–228.

Berthé, D., Choukroune, P. & Jegouzo, P. 1979. Orthogneiss, mylonite and non-coaxial deformation of granites. The example of the South Armorican Shear Zone. *J. Struct. Geol.* **1**, 31–42.

Bouchez, J. L., Lister, G. S. & Nicholas, A. 1983. Fabric asymmetry and shear sense in movement zones. *Geol. Rdsch.* **72**, 401–419.

Crittenden, M. D., Jr., Coney, P. J. & Davis, G. H. (eds.) 1980. *Cordilleran Metamorphic Core Complexes. Mem. geol. Soc. Am.* **153**.

Davis, G. A., Anderson, J. L., Frost, E. G. & Shackelford, T. J. 1980. Mylonitization and detachment faulting in the Whipple–Buckskin–Rawhide Mountains terrane, southeastern California and western Arizona. *Mem. geol. Soc. Am.* **153**, 79–130.

Erskine, B. C. 1985. Mylonite deformation and associated low-angle faulting in the Santa Rosa Mylonite Zone, southern California. Unpublished Ph.D. thesis, University of California at Berkeley.

Erskine, B. C. & Wenk, H.-R. 1985. Evidence for late Cretaceous crustal thinning in the Santa Rosa mylonite zone, southern California. *Geology* **13**, 274–277.

Knopf, E. 1931. Retrogressive metamorphism and phyllonitization. *Am. J. Sci.* **221**, 1–27.

Lipshie, S. R., Oertel, G. & Christie, J. M. 1976. Measurement of preferred orientation of phyllosilicates in schists. *Tectonophysics* **39**, 91–99.

March, A. 1932. Mathematische Theorie der Regelung nach der Korngestalt bei affiner Deformation. *Z. Kristallogr.* **81**, 285–298.

Means, W. D. 1981. The concept of steady-state foliation. *Tectonophysics* **78**, 179–199.

Means, W. D., Williams, P. F. & Hobbs, B. E. 1984. Incremental deformation and fabric development in KCl/mica mixture. *J. Struct. Geol.* **6**, 391–398.

Mecking, H. 1978. Deformation of single crystals. In: *Proc. 5th Int. Conf. Textures of Materials* (edited by Gottstein, G. & Lücke, K.). Springer, Berlin, **1**, 25–44.

O'Brien, D. K. 1985. Strain estimation and sense of shear determination in phyllonites and ultramylonites based on phyllosilicate preferred orientation. Unpublished M.S. thesis, University of California at Berkeley.

Oertel, G. 1970. Deformation of a slaty, lapillar tuff in the Lake District, England. *Bull. geol. Soc. Am.* **81**, 1173–1188.

Oertel, G. 1983. The relationship of strain and preferred orientation of phyllosilicate grains in rocks—a review. *Tectonophysics* **100**, 413–447.

Oertel, G. 1985. Reorientation due to grain shape. In: *Preferred Orientation in Deformed Metals and Rocks. An Introduction to Modern Texture Analysis* (edited by Wenk, H.-R.). Academic Press Inc., Orlando, Florida, 259–265.

Platt, J. P. 1984. Secondary cleavages in ductile shear zones. *J. Struct. Geol.* **6**, 439–442.

Platt, J. P. & Vissers, R. L. M. 1980. Extensional structures in anisotropic rocks. *J. Struct. Geol.* **2**, 397–410.

Ratschbacher, L. 1986. Kinematics of Austro-Alpine cover nappes: changing translation path due to transpression. *Tectonophysics* **125**, 335–356.

Ratschbacher, L. & Klima, K. 1985. Übersicht über Geologie und Mineralgehalt in einem Querprofil vom Altkristallin zur Kalkalpenbasis (Triebener Tauernpass—Flitzenschlucht, Paltental, Steiermark, Österreich). *Geol. Jb. B.-A.* **128**, 151–173.

Rumble, D. & Oertel, G. 1979. Strain and metamorphism: metaclastic rocks from new Hampshire. *J. Geol.* **87**, 69–86.

Sander, B. 1911. Teibewegung und Gefüge in Gesteinen. *Tschermaks Mineral. Petrog. Mitt.* **30**, 281–314.

Sharp, R. V. 1979. Some characteristics of the eastern Peninsular Ranges mylonite zone: analysis of actual fault zones in bedrock. In: *Proceedings, Conference VII, USGS Open File Report* **79–1239**, 258–267.

Simpson, C. & Schmid, S. M. 1983. An evaluation of criteria to deduce the sense of movement in sheared rocks. *Bull. geol. Soc. Am.* **94**, 1281–1288.

Tullis, J., Snoke, A. W. & Todd, V. R. 1982. Penrose Conference Report: significance and petrogenesis of mylonitic rocks. *Geology* **10**, 227–230.

Tollmann, A. 1959. Der Deckenbau der Ostalpen auf Grund der Neuuntersuchung des zentralalpinen Mesozoikums. *Mitt. Ges. Geol. Bergbaustud.* **10**, 1–62.

Von Gosen, W., Haiges, K.-H., Neubauer, F., Pistotnik, J. & Thiedig, F. 1985. Die tektonischen Baueinheiten am Nord- und Westrand der Gurktaler Decke (Österreich). *Geol. Jb. B.-A.* **127**, 693–699.

Voll, G. 1980. Ein Querprofil durch die Schweizer Alpen vom Vierwaldstätter See zur Wurzelzone—Strukturen und ihre Entwicklung durch Deformationsmechanismen wichtiger Minerale. *Neues Jb. Geol. Paläont. Abh.* **160**, 321–335.

Wenk, H.-R. 1985. Measurement of pole figures. In: *Preferred Orientation in Deformed Metals and Rocks. An Introduction to Modern Texture Analysis* (edited by Wenk, H.-R.). Academic Press Inc., Orlando, Florida, 11–47.

White, S. H., Burrows, S. E., Carreras, J., Shaw, N. D. & Humphreys, F. J. 1980. On mylonites in ductile shear zones. *J. Struct. Geol.* **2**, 175–188.